



Contents lists available at ScienceDirect

Journal of Sound and Vibration

journal homepage: www.elsevier.com/locate/jsvi

An experimentally validated piezoelectric nonlinear energy sink for wideband vibration attenuation



Tarcisio M.P. Silva ^a, Marcel A. Clementino ^a, Carlos De Marqui Jr. ^{a, *},
Alper Erturk ^b

^a Department of Aeronautical Engineering, Sao Carlos School of Engineering, University of Sao Paulo, Brazil

^b G.W. Woodruff School of Mechanical Engineering, Georgia Institute of Technology, Atlanta, GA, USA

ARTICLE INFO

Article history:

Received 19 March 2018

Received in revised form 8 August 2018

Accepted 17 August 2018

Available online 5 September 2018

Handling Editor: L. Huang

Keywords:

Nonlinear energy sink

Piezoelectricity

Targeted energy transfer

Vibration attenuation

ABSTRACT

Various researchers have investigated the behavior of a linear mechanical oscillator coupled to a nonlinear mechanical attachment that has essential stiffness nonlinearity. Under certain conditions, the essentially nonlinear attachment acts as a nonlinear energy sink (NES) and one-way energy transfer from the main structure to the nonlinear attachment can be achieved. An important characteristic of an essentially nonlinear attachment is that it does not possess any preferential resonance frequency, resulting in increased robustness against detuning, thereby enabling frequency-wise wideband performance. This work presents an experimentally validated piezoelectric-based NES for wideband vibration attenuation. The electrical circuit consists of a negative capacitance shunt (introduced for cancelling the piezoelectric capacitance) combined in series with a nonlinear capacitance of cubic order that is realized using operational amplifiers. Design and practical implementation of the NES shunt circuit are discussed in detail. The performance of the piezoelectric NES to attenuate vibrations over a wide range of frequencies is numerically simulated and experimentally validated for a cantilever in the absence and presence of tip mass attachments.

© 2018 Elsevier Ltd. All rights reserved.

1. Introduction

The attenuation of undesired structural vibrations is of interest in a variety of engineering applications ranging from industrial machines to aerospace structures. Especially for lightweight and flexible structures used in aircraft and spacecraft systems, piezoelectric shunt damping [1,2] offers remarkable advantages as an electronic damping approach without the mass loading effects of conventional and bulky vibration damping methods [3,4]. In the 1990s, piezoelectric shunt damping was studied for various structures ranging from experimental beam setups [5] to aircraft panels [6,7] and space truss structures [7], yielding successful results. Various types and applications of piezoelectric shunt damping can be found in review articles by Lesieutre [1] and Ahmadian and Deguilio [2].

Piezoelectric shunt damping is applied by connecting an electrical circuit to the electrode terminals of a piezoelectric interface (e.g., patch or stack) that is attached to the main structure. Resistive, capacitive, inductive, and resistive-inductive shunt circuits are the typical linear shunt concepts [1]. The resistive shunting concept was first used by Uchino and Ishii

* Corresponding author.

E-mail address: demarqui@sc.usp.br (C. De Marqui).

[8] and its effect on the structure is analogous to constraint layer damping treatments [1]. Capacitive shunting results in a variation of structural stiffness with changing external capacitance. Changing structural stiffness alters the resonance frequencies of the structure but damping is not affected. Inductive shunting was first studied by Forward [9] and it was shown that the inductance can be tuned to create an undamped dynamic vibration absorber effect. Knowing from Uchino and Ishii [8] that a resistor could be used to create damping effect, Hagood and von Flotow [5] connected a resistor and inductor in series to realize the damped dynamic vibration absorber effect. Wu [10] proposed connecting the resistor and inductor in parallel as an alternative resistive-inductive shunt circuit. The result is again a damped dynamic vibration absorber (or a piezoelectric vibration absorber) but the damping trend with changing shunt resistance is reversed (as compared to the series connection). The resistive-inductive shunt circuits (series or parallel) have received the most attention [1] as they create the damped dynamic vibration absorber effect with proper selection of inductance and resistance.

Linear piezoelectric vibration absorbers, such as the resistive-inductive circuits, are tuned to a specific resonance frequency. Therefore, their control performance may be significantly reduced if the target frequency is modified due to variation of environmental conditions (e.g. temperature), fabrication tolerances, parameter uncertainties, or nonlinearities, among others. To overcome these limitations, dell'Isola et al. [11–13] investigated the multimodal damping of continuous electroelastic systems by distributing piezoelectric elements that are interconnected to a single passive circuit by leveraging the principle of similarity.

Researchers have also explored different types of nonlinear piezoelectric shunt circuits to enhance the vibration suppression bandwidth of piezoelectric absorbers. Piezoelectric semi-passive or semi-active switch shunting techniques introduce nonlinear treatment of the electrical output of piezoelectric elements and induce enhanced damping or stiffness modification in systems with weak electromechanical coupling (see the papers by Guyomar and co-workers [14–17]). Soltani and Kerschen [18] explored the effects of a nonlinear piezoelectric tuned vibration absorber designed to attenuate vibrations of a nonlinear primary system, which is based on the principle of similarity [19]. More recently, Lossouarn et al. [20] presented a fully passive nonlinear piezoelectric resonant shunt using a physical inductor subjected to magnetic saturation that generates a hardening nonlinearity in the electrical domain.

Another type of nonlinear piezoelectric absorber investigated to address the limitations of linear shunt circuits is based on the nonlinear energy sink (NES) concept [21]. A NES is an essentially nonlinear attachment with no preferential resonance frequency, and it offers nonlinear energy pumping (or targeted energy transfer) under certain conditions. This phenomenon, first reported by Gendelman [22–24], leads to one-way transfer of the vibrational energy from a host structure to the NES, where this energy is localized and dissipated. To the best of our knowledge, Viguié et al. [25] presented the first numerical investigation of a piezoelectric-based energy sink. Although the authors also discussed an experimental setup, only numerical results were reported in their publication. More recently, Zhou et al. [26] presented an essentially nonlinear shunt circuit for the realization of a piezoelectric NES applied to mistuned bladed disks. Although relevant numerical analyses and discussions have been presented [25,26], a nonlinear circuit that allows practical implementation of a piezoelectric NES has not been covered in the literature.

This paper presents an experimentally validated piezoelectric NES for vibration attenuation. An essentially nonlinear piezoelectric shunt circuit is designed to provide the required nonlinearity. The circuit parameters are obtained from the Rayleigh-Ritz model of a thin cantilever with piezoelectric layers for the first bending mode. First, the essentially nonlinear behavior of the circuit is experimentally verified. Then the effects of the nonlinear shunt circuit on the resonance of the first bending mode of an electromechanically coupled beam with a tip mass are numerically demonstrated and experimentally validated. The robustness of the piezoelectric NES against detuning is confirmed when various tip masses are added to the cantilever to alter the fundamental resonance frequency.

2. Piezoelectric nonlinear energy sink coupled to a linear structure

2.1. Theory

Fig. 1 presents the schematic of an electromechanically coupled cantilever partially covered by two layers of piezoelectric material (bimorph in parallel configuration). The electrode pairs are connected to a shunt circuit (which is depicted as a standard linear resonant shunt in Fig. 1a and an essentially nonlinear circuit in Fig. 1b). The equations of motion of electromechanically coupled beams combined to linear electrical circuits [27] and also to nonlinear electrical circuits, such as the piezoelectric-based NES [26], have been presented in the literature and are briefly revisited in this section.

The electromechanically coupled beam combined with a linear shunt circuit is first discussed. A resonant circuit in the form of a resistive-inductive (RL) shunt in series presented in Fig. 1a is considered. The governing equations of the electromechanically coupled system are given by

$$m\ddot{x} + c\dot{x} + \left(k^{SC} + \frac{\theta\theta^t}{C_p}\right)x + \frac{\theta}{C_p}q = F \quad (1)$$

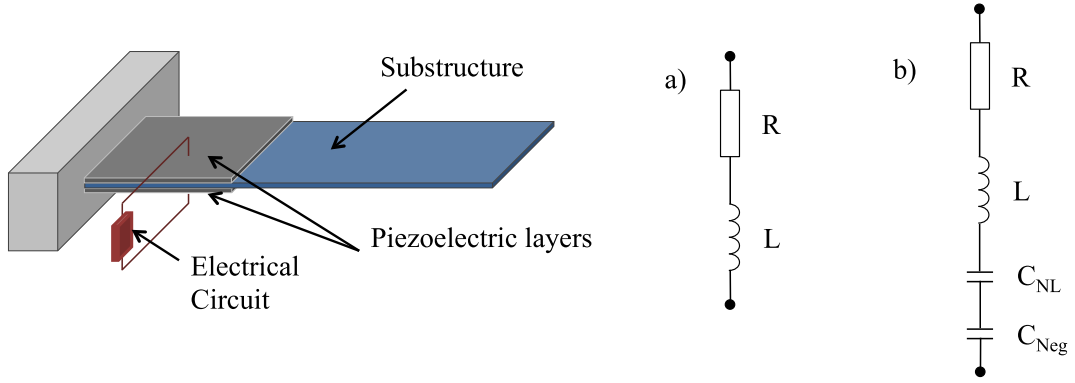


Fig. 1. Electromechanically coupled cantilever with piezoelectric layers shunted to (a) linear resonant circuit and (b) essentially nonlinear circuit.

$$L\ddot{q} + R\dot{q} + \frac{1}{C_p}q + \frac{\theta^t}{C_p}x = 0 \quad (2)$$

where m is the mass of the beam, c is the damping coefficient, k^{SC} is the short-circuit stiffness of the cantilever, θ is the electromechanical coupling, C_p is the equivalent capacitance, q is the electrical charge flowing from the piezoelectric layers, and F stands for the external force vector acting on the system. Note that the terms in the governing equations can be scalar (in which case the transpose of the electromechanical coupling is itself) or matrices as in the Rayleigh-Ritz model implemented in this work. When the inductor and resistor are properly adjusted [5,28,29] significant vibration attenuation is achieved although the frequency bandwidth of such passive circuit is quite narrow. Furthermore, for low-frequency vibration attenuation in flexible structures, the inductance requirement can be very large.

The circuit configuration of Fig. 1b [26] introduces nonlinearity to the system through a nonlinear capacitance (C_{NL}). Zhou et al. [26] suggest the use of ferroelectric capacitors to introduce nonlinearity to the electromechanical system. The nonlinear voltage-charge characteristic of ferroelectric capacitors is usually close to a third degree polynomial. However, the linear term of the third order polynomial and the internal capacitance of piezoelectric material hinder the realization of essential nonlinearity. A negative capacitance (C_{Neg}) in series with both the nonlinear capacitor and the internal capacitance of piezoelectric material enables minimization (ideally elimination) of the linear voltage-charge behavior.

The governing equations of the electromechanically coupled cantilever combined with the essentially nonlinear circuit in Fig. 1b are

$$m\ddot{x} + c\dot{x} + \left(k^{SC} + \frac{\theta\theta^t}{C_p}\right)x + \frac{\theta}{C_p}q = F \quad (3)$$

$$\varepsilon L_{opt}\ddot{q} + \beta R_{opt}\dot{q} + \frac{1}{C_{Res}}q + \alpha q^3 + \frac{\theta^t}{C_p}x = 0 \quad (4)$$

where ε and β are adjusting parameters for the nonlinear case since Equation (4) uses the optimum tuning parameters of the linear resonant shunt (L_{opt} and R_{opt}) as reference (see for instance [5,28,29]), C_{Res} is a residual capacitance related to negative and piezoelectric capacitances and α is a constant. Another parameter (μ) accounts for the effect of negative capacitance through the expression $1/C_{Res} = \mu/C_p$. The proper combination of the parameters α , ε , β , and μ leads to enhanced vibration attenuation. When $\varepsilon = 1$, $\beta = 1$, $\mu = 1$, and $\alpha = 0$ the RL in series case is obtained. Moreover, in the above formulation, as discussed by Zhou et al. [26], the parameter ε is usually much smaller than one, leading to inductance values substantially smaller than those typically used in RL circuits.

This work uses a variational formulation, by combining Hamilton's principle with the Rayleigh-Ritz method to model the electromechanically coupled cantilever of Fig. 1 based on the Euler-Bernoulli beam assumptions. Derivation details are omitted in the present paper since this type of modeling approach has been well covered in the literature [30]. In this framework, the piezoelectric and geometric nonlinearities [31,32] are assumed to be negligible; however, such additional terms can be included and be compensated for in the electrical domain with additional circuit components [33].

2.2. Essentially nonlinear circuit implementation

This section presents an essentially nonlinear piezoelectric shunt circuit as well as its practical implementation prior to experimental validation. The nonlinear circuit is designed to accomplish the functions discussed in Fig. 1b. As mentioned previously, in a recent effort [26], nonlinear ferroelectric capacitance was proposed to introduce essential nonlinearity to the

system. Nonlinear capacitors present nonlinear voltage-charge behavior usually close to a third order polynomial [34], and relying on the nonlinearity of the ferroelectric capacitor [26] is a relatively limited approach since the inherent cubic nonlinearity cannot be tailored easily. Here, we present a circuit configuration to introduce exclusively cubic voltage-charge behavior.

Fig. 2 displays the nonlinear circuit proposed in this work. The piezoelectric material is connected to a resistor R_1 and inductor L_1 , providing electrical analogous of damping and inertia, respectively. A negative capacitance circuit is also connected in series to the piezoelectric material to minimize the linear voltage-charge term in Equation (4). The bottom part of the circuit has a series of operational amplifiers and two multipliers (AD633) to obtain the cubic voltage-charge behavior.

In the circuit of Fig. 2, the negative capacitance is obtained from,

$$C_{neg} = -\frac{R_{a4}C_2}{R_{a3}} \tag{5}$$

where $R_{a3} = R_{a3c} + R_{a3m}$ and the subscript c stands for “complementary” and the subscript m stands for “measurement”.

The voltage across the resistor R_{a3m} ($V_{meas} = V_c - V_2$) is the reference to obtain the cubic term of the essentially nonlinear circuit ($V_c = \alpha q_p^3$). The voltages V_2 and V_c are measured with the operational amplifiers OA2 and OA3, respectively, and driven to the voltage amplifier (OA4, R_{a1} and R_{a2}) that provides $V_{meas} = V_c - V_2$. The voltage output of OA4 is proportional to the current flowing in R_{a3m} that is also proportional to the charge flowing from the piezoelectric layers. Therefore,

$$V_{meas} = V_c - V_2 = R_{a3m}\dot{q}_2 = \frac{R_{a3m}}{R_{a4}C_2}q_p \tag{6}$$

which is driven to the voltage amplifier (OA5, R_{a1} and R_{a2}) to adjust the voltage input of the multipliers. The voltage output of each multiplier (AD633) is defined as

$$V_{q2} = \frac{V_{amp}^2}{10} \tag{7}$$

and

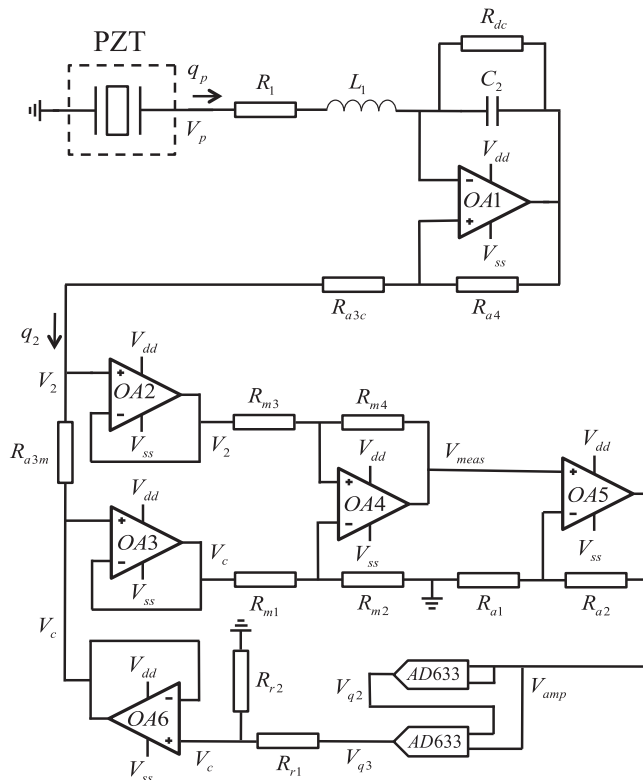


Fig. 2. Nonlinear electrical circuit representing an electrical NES.

$$V_{q3} = \frac{V_{q2} V_{amp}}{10} \quad (8)$$

where the factor 1/10 is due to the multiplier. The cubic voltage–charge characteristic is then obtained in the divider circuit (R_{r1} and R_{r2}) as

$$V_c = \frac{R_{r2}}{R_{r1} + R_{r2}} \left(1 + \frac{R_{a2}}{R_{a1}}\right)^3 \frac{1}{100} \frac{R_{a3m}^3}{(R_{a4} C_2)^3} q_p^3 \quad (9)$$

adding the essential nonlinearity to the circuit. The resistance of R_{r2} is obtained from,

$$R_{r2} = R_{r1} \frac{\gamma}{1 - \gamma} \quad (10)$$

where

$$\gamma = \frac{R_{a1}^3}{(R_{a1} + R_{a2})^3} 100 \frac{(R_{a4} C_2)^3}{R_{meas}^3} \alpha \quad (11)$$

and the value of R_{r1} can be chosen arbitrarily. The resistors R_{a1} and R_{a2} should be calculated according to the saturation voltage of the voltage multipliers.

As a major advantage, the proposed piezoelectric NES circuit can easily be modified by changing a few electrical components. For example, the nonlinear coefficient of cubic stiffness term (α) in Equation (4) can be modified by changing the resistors R_{r1} and R_{r2} . It is also important to note that various nonlinear piezoelectric absorbers (and various other nonlinearities, e.g. Duffing-type) can be achieved through simple modifications to the circuit presented in Fig. 2. Polynomial nonlinearities of virtually any order can be obtained by excluding negative capacitance and adding more multipliers, yielding tuned nonlinear vibration absorbers discussed in the literature [18].

3. Model simulations and experimental validations

This section explores the practical realization of a piezoelectric NES by combining the essentially nonlinear piezoelectric shunt circuit of Section 2 with an electromechanically coupled cantilever. A Rayleigh–Ritz model [30], based on the Euler–Bernoulli beam assumptions, is employed to obtain the modal parameters of the cantilever presented in Fig. 3. Simulations that combine the modal solution of the governing equations (Equations (3) and (4)) with the nonlinear circuit (Fig. 2) in MATLAB Simulink, by using the Simscape Electronics™, are performed to obtain the nonlinear circuit parameters. After that, experimental characterization of the essential nonlinearity provided by the nonlinear shunt circuit is presented. Numerical and experimental results of the electromechanically beam with a tip mass in open- and short-circuit conditions as well as combined to the NES circuit are also presented for various tip mass cases.

Simulations of the clamped beam connected to the nonlinear circuit are carried out using the block diagram of Fig. 3. In this model, the gains m^{-1} , $m^{-1}k$, $m^{-1}c$ are matrices while the acceleration, velocity and displacement (\ddot{x} , \dot{x} and x respectively), and $m^{-1}\theta$ are vectors in the Rayleigh–Ritz model (10 Ritz modes are considered in all numerical simulations). As displayed in

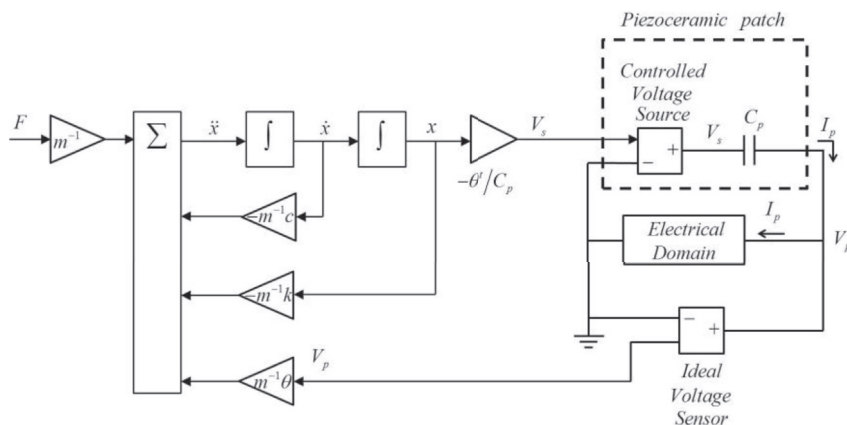


Fig. 3. System level diagram used for numerical simulations of the beam with piezoelectric interface connected to NES circuit.

Fig. 3, the piezoceramic patch is modeled as a controlled voltage source connected in series with the linear capacitor C_p . The piezoceramic is connected in series with the “Electrical domain” block which represents a generic piezoelectric circuit (e.g. RL or NES). The block diagram model of Fig. 3 is based on the system level approach presented by Elvin [35].

Fig. 4 displays the experimental setup for the cantilever with NES circuit under harmonic base excitation. In such case, the excitation is due to the inertia of the structure and, therefore, $F = m^* a_b$ in Equations (1) and (3) as well as in the block diagram of Fig. 3, where a_b is the base acceleration and m^* is the mass per length of the beam in the absence of a tip mass (and is modified in the presence of a tip mass). An accelerometer is employed to measure base acceleration and a laser Doppler vibrometer measures the tip velocity. The essentially nonlinear piezoelectric shunt circuit is also displayed in Fig. 3. Two piezoelectric patches (QP10N from Midé Corporation) are bonded to the clamped end of the beam in the form of a bimorph. The piezoceramic patches are connected in parallel and the resulting capacitance is 106 nF. The geometric and material properties of the beam as well as the electromechanical properties of the piezoelectric material (PZT-5A) are given in Table 1, which were employed in the simulations.

3.1. Nonlinear shunt circuit parameters

The parameters of the nonlinear shunt circuit are numerically obtained from time domain simulations using the block diagram of Fig. 3. As discussed in Section 2, Equation (4) uses the tuning parameters of the linear resonant shunt (L_{opt} and R_{opt}) as reference. The literature includes different approaches to obtain the optimum parameters of linear resonant shunt circuits (see for instance [5,28,29]). In this work, however, since a NES is not tuned to any specific frequency, the inductance (in the resistive-inductive in series shunt circuit) is estimated as $1/\omega_{sc}^2 C_p$ (where ω_{sc} is the resonance frequency of the target mode), while the optimal resistance converts the original peak to a *plateau* without generating two new modes. If one uses slightly different values of inductance and resistance as reference, different parameters for the nonlinear circuit will be obtained (although the performance of the NES will be quite similar). The parameters calculated for the linear shunt circuit are presented in Table 2, along with the critical nonlinear coefficient (α_c) of Equation (4) defined as a function of the maximum electrical charge flowing from the piezoelectric layers in the RL shunt case.

The procedure to obtain the NES parameters in Equation (4) (α , ε , β and μ) is as follows: Initially, the parameter μ is assumed to be extremely low (eliminating the effects of the linear capacitance as expected in an ideal case). Then, time domain simulations are performed for a range of values of α , ε and β , searching for the combination that yields enhanced vibration attenuation. However, such low values of μ assumed in the simulations would lead to system instability in practice (due to a strong cancelation of the linear capacitance, C_p), which is not observed in simulations since ideal electrical elements are assumed in the model. Therefore, experimental tests are also conducted to obtain the smallest value of μ that can be used in a physical setting. For these experiments the breadboard implementation of the circuit shown in Fig. 5 is employed. In the circuit, $R_1 = \beta R_{lin}$ and $L_1 = \varepsilon L_{lin}$ are the NES resistor and inductor, respectively. The resistor R_{a3} is a potentiometer whose resistance is changed (changing the value of μ) in order to determine the smallest value of μ without instability, which is then used in NES simulations (along with the optimal parameters α , ε , and β) and validation experiments.

The resulting nonlinear parameters, previously defined in Equation (4), are given in Table 3. An important characteristic of NES is that the inductance of the nonlinear circuit is two orders of magnitude smaller than the inductance of the linear RL case (Table 2). The set of electrical components presented in Table 4 were calculated using the equations presented in Section 2.2 and allows the practical realization of an essentially nonlinear shunt circuit whose parameters are given in Table 3.

3.2. Experimental characterization of the nonlinear shunt circuit

Considering the electrical elements displayed in Table 4, the experimental characterization of the essential nonlinearity provided by the nonlinear shunt circuit is presented first. The characterization of the nonlinear shunt circuit is performed by

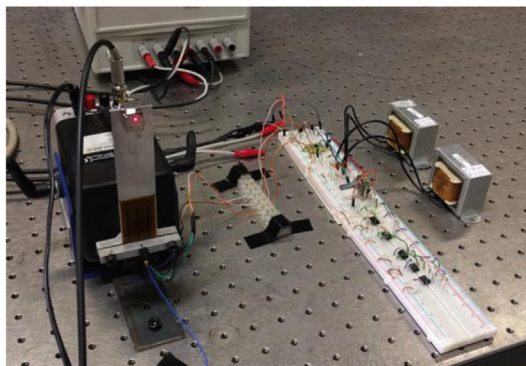


Fig. 4. Experimental setup showing the cantilever and the NES circuit.

Table 1
Geometrical and material properties of the cantilever beam and PZT5A.

Length of the beam (mm)	118.8	Length of the PZT (mm)	39.3
Width of the beam (mm)	27.8	Width of the PZT (mm)	20.6
Thickness of the beam (mm)	1.0	Thickness of the PZT (mm)	0.24
Young's Modulus of the beam (GPa)	70.0	Young's Modulus of the PZT (GPa)	67.0
Mass density of the beam (kg/m ³)	2700.0	Mass density of the PZT (kg/m ³)	7750.0
Permittivity ϵ_{33} of the PZT (nF/m)	1800.0	Piezoelectric constant d_{31} (pm/V)	-171.0

Table 2
Parameters obtained from the reference case (RL shunt in series).

L_{lin}	R_{lin}	$\alpha_c = 1/C_p \max(Q_p)^2$	$\max(Q_p)$	ω_{sc}
363.6H	16.5 k Ω	$9.8 \times 10^{16} \text{ V/C}^3$	$9.81 \times 10^{-6} \text{ C}$	25.19 Hz

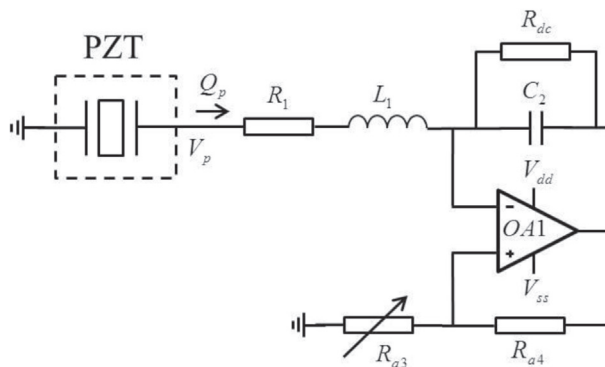


Fig. 5. Circuit employed for the experimental determination of μ .

exciting (harmonic base excitation) the same cantilever of Section 3.1 (with a tip mass of 22.9 g) at the short circuit resonance frequency (25.19 Hz). Since the electrical elements of the circuit are known, the measurement of voltages at specific points allows the calculation of the electrical charge. The goal is to compare the negative capacitance to the equivalent capacitance of the bimorph as well as experimentally verify the cubic voltage-charge characteristic of the circuit.

Fig. 6 displays the contribution of different parts of the circuit measured during the experiments. The voltages were directly measured at the relevant points of the circuit and charge obtained from corresponding equations. It is noteworthy in Fig. 6a that the magnitude of the negative capacitance is quite similar to the equivalent capacitance of the bimorph. The slope of linear voltage-charge trend of the piezoelectric material is $8.3 \times 10^6 \text{ V/C}$ while the slope of voltage-charge trend of negative capacitance is $-8.1 \times 10^6 \text{ V/C}$. Therefore, the residual linear stiffness is less than 2.5% of the original linear stiffness of the system (piezoelectric capacitance). The resulting capacitance of the system is negligible since the achieved μ parameter (Equation (4)) is 0.2. Note that a negative capacitance value larger than the achieved one would lead to circuit instability (as discussed in Section 3.1).

Fig. 6b displays the nonlinear voltage-charge behavior (which is analogous to the nonlinear restoring elastic force of a mechanical NES) induced by the nonlinear circuit with and without the residual capacitance of piezoelectric layers. The measured voltage-charge relation can be approximated by a cubic term αq^3 (as in Equation (4)) with $\alpha = 1.8 \times 10^{17} \text{ V/C}^3$. Therefore, the circuit of Fig. 2 provides essential nonlinearity. Although a residual capacitance is present, the experimental results in the next section reveal that it is sufficiently small to enable a good performance over a wide range of frequencies.

3.3. Numerical simulations and experimental validation of the piezoelectric NES

This section presents numerical simulations and experimental validation of the piezoelectric NES. The simulations use the block diagram of Fig. 3 with data provided in Tables 1 and 4 while the experimental setup is the one described in Fig. 4. In order to confirm the robustness of the piezoelectric NES to detuning, simulations and experiments are performed for different tip mass values while the same nonlinear circuit parameters presented in Table 4 are considered in all cases (simulations and experiments). Controlled base acceleration was considered in the experiments in a feedback setting.

Fig. 7 shows the frequency response of tip velocity for the first mode of the beam for two different tip mass values (22.9 g in Fig. 7a and 15.0 g in Fig. 7b) and base acceleration of 0.04 g. The short-circuit, open-circuit, and NES circuit cases are displayed. The continuous lines stand for the model simulation results while the round markers are the experimental data.

Table 3
NES parameters used in the numerical simulations.

α/α_{crit}	$\epsilon = L_1/L_{lin}$	$\beta = R_1/R_{lin}$	$\mu = C_p/C_{res}$
1.565	0.0138	0.666	0.128

Table 4
Electrical components of the NES circuit.

Component	Value	Component	Value
L_1	5H	R_1	11 k Ω
R_{dc}	500 k Ω	C_2	672 nF
R_{a4}	10 k Ω	R_{a3m}	15 k Ω
R_{a3c}	40 k Ω	R_m	1 M Ω
R_{a1}	100 k Ω	R_{a2}	39.1 k Ω
R_{r1}	1 M Ω	R_{r2}	1.05 M Ω

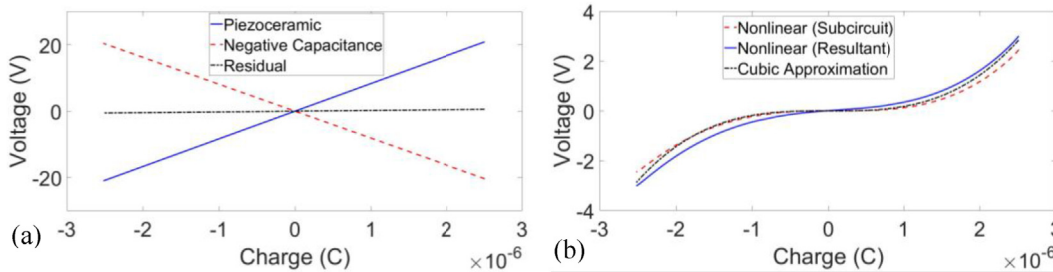


Fig. 6. Experimental characterization of the essentially nonlinear circuit: (a) contribution of different parts of the circuit and (b) nonlinear voltage-charge behavior.

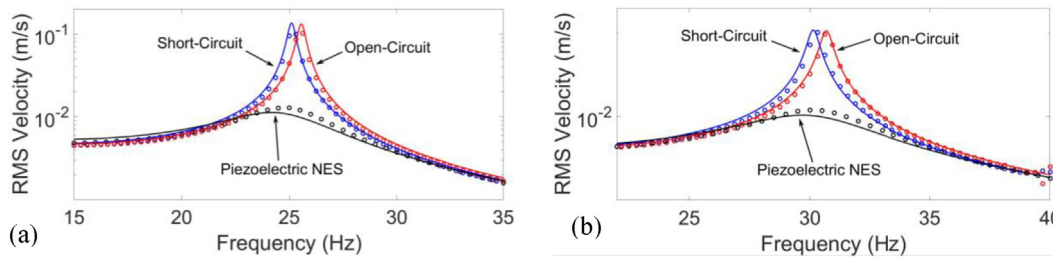


Fig. 7. Model simulations (continuous lines) and experimental data (round markers) for the frequency response of the beam under harmonic base excitation (base acceleration 0.04 g) for short-circuit condition, open-circuit condition, and piezoelectric NES for a tip mass of (a) 22.9 g and (b) 15.0 g.

The overall agreement between the numerical and experimental results in Fig. 7 is very good. It should be noted that ideal electrical elements were considered in the simulations while commercially available resistors and capacitors may have capacitances and resistances slightly different from the calculated ones due to manufacturing tolerance issues and other. Additionally, in practice, op-amps are not ideal electrical elements (unlike in simulations) since they exhibit output resistance. These are the sources of minor differences observed in Fig. 7 between model simulations and experimental data. At the short circuit resonant frequency of the cantilever for both tip mass scenarios (22.9 g and 15.0 g), the tip velocity of the electromechanically coupled cantilever with the NES circuit is around 90% less than that of the beam in short circuit condition, showing that the piezoelectric NES is insensitive to frequency variations.

Simulations and experiments were also performed for smaller tip mass value (7.7 g) and in the absence of a tip mass. In all cases, the same nonlinear shunt circuit considered in Fig. 7 was employed to check the performance of the NES over a broad range of frequencies. Fig. 8a and b display the tip velocity for 7.7 g and absence of tip mass, respectively. The base acceleration was increased to 0.16 g and 0.24 g, respectively, to increase the excitation intensity. At the short circuit resonance of each case, piezoelectric NES provides a tip velocity 85% and 70% less than that of the short circuit condition of each case.

As a final discussion, Fig. 9 shows the time history of the product of cantilever tip velocity and piezoelectric voltage output for an example case of using NES. This product is proportional to power flow from the mechanical domain to the electrical

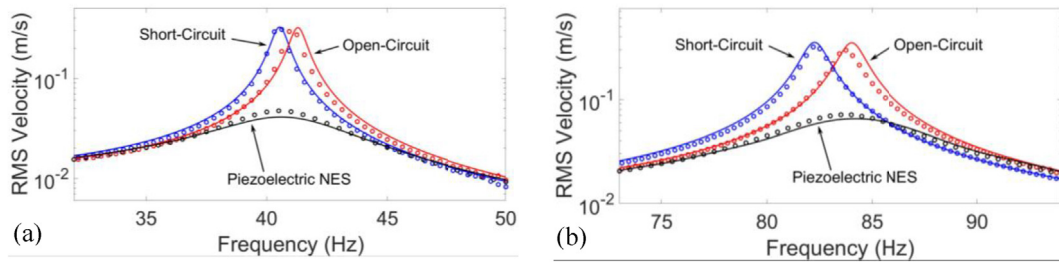


Fig. 8. Model simulations (continuous lines) and experimental data (round markers) for the frequency response of the beam under harmonic base excitation for short-circuit condition, open-circuit condition, and piezoelectric NES for a tip mass of (a) 7.7 g (base acceleration 0.16 g) and (b) in the absence of a tip mass (base acceleration 0.24 g).

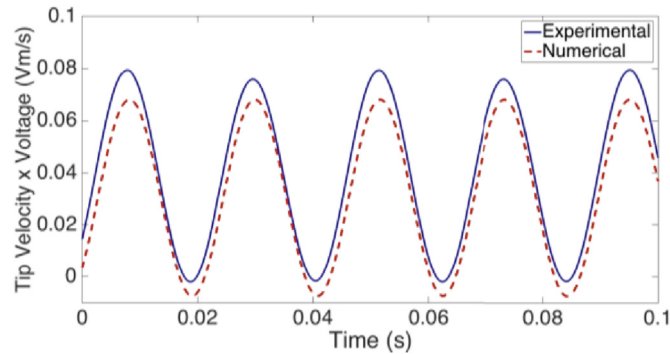


Fig. 9. Time series of the product of tip velocity and piezoelectric voltage output (experimental data for excitation at the short-circuit resonance frequency for the cantilever with 22.9 g tip mass).

domain of the system.¹ The time series were obtained for the cantilever with a tip mass of 22.9 g harmonically excited around its short circuit resonance frequency. Fig. 9 shows that power flows from the mechanical to the electrical domain (in agreement with positive power due to damping in the governing equations) predominantly in a one-way fashion, further confirming the NES behavior.

4. Conclusions

An experimentally validated piezoelectric NES was presented. The essentially nonlinear piezoelectric shunt combines a resistor, an inductor, and two operational amplifier (op-amp) and multiplier based sub-circuits: (1) negative capacitance circuit and (2) essential nonlinear circuit. The negative capacitance is employed to cancel the internal capacitance of piezoelectric material. Very limited literature on the subject suggests the use of ferroelectric capacitors to provide the cubic voltage-charge characteristic for piezoelectric NES implementation. However, relying on the nonlinearity of the ferroelectric capacitor is a relatively limited approach in that the cubic nonlinearity cannot be tailored easily. The op-amp-based essential nonlinear circuit presented in this work provides exclusively cubic voltage-charge characteristic to the system. Moreover, different nonlinearities can also be achieved through simple modifications to the circuit.

The effects of the NES over the elastic behavior of an electromechanically coupled cantilever were first investigated. The modal parameters of the beam were obtained from a Rayleigh-Ritz solution and combined with the nonlinear shunt circuit in MATLAB Simulink. Preliminary simulations were first performed in order to adjust the nonlinear shunt circuit parameters. The behavior of the beam under harmonic base excitation was then discussed for the short- and open-circuit conditions as well as combined with the NES circuit. Significant vibration attenuation was observed over a wide range of frequencies when different tip mass values were considered.

The nonlinear characteristics of the circuit were also experimentally validated. The obtained negative capacitance magnitude was very close to the internal capacitance of piezoelectric layers added to the beam. The resultant coefficient of the linear term was 98% smaller than that without negative capacitance. This is an important feature since essential nonlinearity

¹ Note that, if Equation (3) is written in terms of voltage, the power associated with electromechanical coupling becomes $-\theta V_p \dot{x}$, which is ensured to be positive when the phase between voltage and velocity is 0° since θ is negative.

is required for one-way energy transfer. The cubic voltage-charge characteristic added by the nonlinear circuit was also experimentally validated and it could be properly approximated by a cubic term.

The effects of the NES over the first resonance of an electromechanically coupled beam were investigated. The time history of the product of tip velocity and piezoelectric voltage shows the one-way energy flow from mechanical to electrical domain for a certain tip mass added to the beam. Moreover, the NES was also validated for different tip mass values. Vibration attenuation was observed for a wide range of frequencies (22.5 Hz–84.0 Hz). Although the performance decays with increasing frequency, a behavior already numerically reported in the literature, significant attenuation is observed over the wide range of frequencies, showing that the proposed piezoelectric NES is robust against detuning.

Acknowledgements

The authors acknowledge the support from CNPq (grant 402160/2013-4) and also São Paulo Research Foundation (FAPESP) grant# 2013/15264-3.

Appendix A. Supplementary data

Supplementary data related to this article can be found at <https://doi.org/10.1016/j.jsv.2018.08.038>.

References

- [1] G.A. Lesiutre, Vibration damping and control using shunted piezoelectric materials, *Shock Vib. Digest* 30 (1998) 187–195, <https://doi.org/10.1177/058310249803000301>.
- [2] M. Ahmadian, A.P. DeGiulio, Recent advances in the use of piezoceramics for vibration suppression, *Shock Vib. Digest* 33 (2001) 15–22.
- [3] A.D. Nashif, D.I.G. Jones, J.P. (John P.) Henderson, *Vibration Damping*, Wiley, 1985.
- [4] D.I.G. Jones, *Handbook of Viscoelastic Vibration Damping*, J. Wiley, 2001. <https://www.wiley.com/en-us/Handbook+of+Viscoelastic+Vibration+Damping-p-9780471492481>. (Accessed 23 January 2018).
- [5] N.W. Hagood, A. von Flotow, Damping of structural vibrations with piezoelectric materials and passive electrical networks, *J. Sound Vib.* 146 (1991) 243–268, [https://doi.org/10.1016/0022-460X\(91\)90762-9](https://doi.org/10.1016/0022-460X(91)90762-9).
- [6] S. Wu, Piezoelectric shunt vibration damping of an F-15 panel under high-acoustic excitation, *Proc. SPIE* 3989 (2000) 276–287, <https://doi.org/10.1117/12.384568>.
- [7] N.W. Hagood, E.F. Crawley, Experimental investigation of passive enhancement of damping for space structures, *J. Guid. Contr. Dynam.* 14 (1991) 1100–1109, <https://doi.org/10.2514/3.20763>.
- [8] K. Uchino, T. Ishii, Mechanical damper using piezoelectric ceramics, *J. Ceram. Soc. Japan* 96 (1988) 863–867, <https://doi.org/10.2109/jcersj.96.863>.
- [9] R.L. Forward, Electronic damping of vibrations in optical structures, *Appl. Optic.* 18 (1979) 690, <https://doi.org/10.1364/AO.18.000690>.
- [10] S. Wu, Piezoelectric shunts with a parallel R-L circuit for structural damping and vibration control, in: C.D. Johnson (Ed.), *Proc. Vol. 2720, Smart Struct. Mater. 1996 Passiv. Damping Isol.*, International Society for Optics and Photonics, 1996, pp. 259–269, <https://doi.org/10.1117/12.239093>.
- [11] S. Alessandroni, F. Dell'Isola, M. Porfiri, A revival of electric analogs for vibrating mechanical systems aimed to their efficient control by PZT actuators, *Int. J. Solid Struct.* 39 (2002) 5295–5324, [https://doi.org/10.1016/S0020-7683\(02\)00402-X](https://doi.org/10.1016/S0020-7683(02)00402-X).
- [12] U. Andreaus, F. Dell'isola, M. Porfiri, Piezoelectric passive distributed controllers for beam flexural vibrations, *JVC/J. Vib. Control* 10 (2004) 625–659, <https://doi.org/10.1177/1077546304038224>.
- [13] S. Alessandroni, U. Andreaus, F. Dell'Isola, M. Porfiri, A passive electric controller for multimodal vibrations of thin plates, *Comput. Struct.* 83 (2005) 1236–1250, <https://doi.org/10.1016/j.compstruc.2004.08.028>.
- [14] C. Richard, D. Guyomar, D. Audigier, G. Ching, Semi-passive damping using continuous switching of a piezoelectric device, in: T.T. Hyde (Ed.), *International Society for Optics and Photonics*, 1999, pp. 104–111, <https://doi.org/10.1117/12.349773>.
- [15] C. Richard, D. Guyomar, D. Audigier, H. Bassaler, Enhanced semi passive damping using continuous switching of a piezoelectric device on an inductor, in: *Proc. SPIE - Int. Soc. Opt. Eng.*, 2000, pp. 288–299, <https://doi.org/10.1117/12.384569>.
- [16] M. Lallart, L. Yan, C. Richard, D. Guyomar, Damping of periodic bending structures featuring nonlinearly interfaced piezoelectric elements, *J. Vib. Contr.* (2015) 1–12, <https://doi.org/10.1177/1077546314567724>.
- [17] D. Guyomar, M.E. Lallart, T. Monnier, Stiffness tuning using a low-cost semiactive nonlinear technique, *IEEE/ASME Trans. Mechatron.* 13 (2008) 604–607, <https://doi.org/10.1109/TMECH.2008.2004411>.
- [18] P.S. Soltani, G. Kerschen, The nonlinear piezoelectric tuned vibration absorber, *Smart Mater. Struct.* 24 (2015), <https://doi.org/10.1088/0964-1726/24/7/075015>.
- [19] G. Habib, G. Kerschen, A principle of similarity for nonlinear vibration absorbers, *Phys. D Nonlinear Phenom.* 332 (2016) 1–8, <https://doi.org/10.1016/j.physd.2016.06.001>.
- [20] B. Lossouarn, J.-F. Deü, G. Kerschen, A fully passive nonlinear piezoelectric vibration absorber, *Philos. Trans. R. Soc. A* 376 (2018), 20170142, <https://doi.org/10.1098/rsta.2017.0142>.
- [21] A.F. Vakakis, O.V. Gendelman, L.A. Bergman, D.M. McFarland, G. Kerschen, Y.S. Lee, Nonlinear Targeted Energy Transfer in Mechanical and Structural Systems, 2008, <https://doi.org/10.1007/978-1-4020-9130-8>.
- [22] O.V. Gendelman, Transition of energy to a nonlinear localized mode in a highly asymmetric system of two oscillators, *Nonlinear Dynam.* 25 (2001) 237–253, <https://doi.org/10.1023/A:1012967003477>.
- [23] O. Gendelman, L.I. Manevitch, A.F. Vakakis, R. M'Closkey, Energy pumping in nonlinear mechanical oscillators: Part I—dynamics of the underlying Hamiltonian systems, *J. Appl. Mech.* 68 (2001) 34, <https://doi.org/10.1115/1.1345524>.
- [24] A.F. Vakakis, O. Gendelman, Energy pumping in nonlinear mechanical oscillators: Part II—resonance capture, *J. Appl. Mech.* 68 (2001) 42, <https://doi.org/10.1115/1.1345525>.
- [25] R. Vigué, G. Kerschen, M. Ruzzene, Exploration of nonlinear shunting strategies as effective vibration absorbers, *Proc. SPIE, Act. Passiv. Smart Struct. Integr. Syst.* 7288 (2009) 72882B, <https://doi.org/10.1117/12.815805>.
- [26] B. Zhou, F. Thouverez, D. Lenoir, Essentially nonlinear piezoelectric shunt circuits applied to mistuned bladed disks, *J. Sound Vib.* 333 (2014) 2520–2542, <https://doi.org/10.1016/j.jsv.2013.12.019>.
- [27] A. Erturk, D.J. Inman, *Piezoelectric Energy Harvesting*, John Wiley & Sons, Ltd, Chichester, UK, 2011, <https://doi.org/10.1002/9781119991151>.
- [28] K. Yamada, H. Matsuhisa, H. Utsuno, K. Sawada, Optimum tuning of series and parallel LR circuits for passive vibration suppression using piezoelectric elements, *J. Sound Vib.* 329 (2010) 5036–5057, <https://doi.org/10.1016/j.jsv.2010.06.021>.
- [29] P. Soltani, G. Kerschen, G. Tondreau, A. Deremaeker, Piezoelectric vibration damping using resonant shunt circuits: an exact solution, *Smart Mater. Struct.* 23 (2014), <https://doi.org/10.1088/0964-1726/23/12/125014>.

- [30] N.G. Elvin, A.A. Elvin, A general equivalent circuit model for piezoelectric generators, *J. Intell. Mater. Syst. Struct.* 20 (2009) 3–9, <https://doi.org/10.1177/1045389X08089957>.
- [31] S.C. Stanton, A. Erturk, B.P. Mann, D.J. Inman, Resonant manifestation of intrinsic nonlinearity within electroelastic micropower generators, *Appl. Phys. Lett.* 97 (2010), <https://doi.org/10.1063/1.3530449>.
- [32] S. Leadenham, A. Erturk, Unified nonlinear electroelastic dynamics of a bimorph piezoelectric cantilever for energy harvesting, sensing, and actuation, *Nonlinear Dynam.* 79 (2014) 1727–1743, <https://doi.org/10.1007/s11071-014-1770-x>.
- [33] T.M.P. Silva, M.A. Clementino, A. Erturk, C. De Marqui Jr., Equivalent electrical circuit framework for nonlinear and high quality factor piezoelectric structures, *Mechatronics* 54 (October 2018) 133–143.
- [34] E. Gluskin, The use of non-linear capacitors, *Int. J. Electron.* 58 (1985) 63–81, <https://doi.org/10.1080/00207218508939003>.
- [35] N.G. Elvin, Equivalent electrical circuits for advanced energy harvesting, *J. Intell. Mater. Syst. Struct.* 25 (2014) 1715–1726, <https://doi.org/10.1177/1045389X14521878>.